Progress In Electromagnetics Research, Vol. 186, 40–51, 2026

(Received 18 June 2026, Accepted 13 August 2026, Scheduled 7 September 2026)

High-Efficiency Amorphous-Silicon/Silicon-Nitride Grating Couplers for O- and C-Band Photonic Integrated Circuits

William Fraser[1,2,†], Pavel Cheben[2,*], Jens H. Schmid[2], Jianhao Zhang[2], Radovan Korček[2], Shurui Wang[2], Martin Vachon[2], Rubin Ma[2], Daniel Benedikovič[3], Thalía D. Bucio[4], Valerio Vitali[4,5], Frederic Y. Gardes[4], and Winnie N. Ye[1]

[1]*Silicon Micro/NanoPhotonics Group, Carleton University, Ottawa, Canada*
[2]*National Research Council of Canada, Ottawa, Canada*
[3]*Department of Multimedia and Information-Communication Technologies, University of Žilina, Žilina, Slovakia*
[4]*Optoelectronics Research Centre, Highfield Campus, University of Southampton, Southampton, UK*
[5]*Electrical, Computer, and Biomedical Engineering Department, University of Pavia, Pavia, Italy*

ABSTRACT: Silicon nitride (Si_3N_4) has emerged as a compelling platform for visible-light, quantum-photonic, and nonlinear-optical applications because of its broad transparency window, low propagation loss, and negligible two-photon absorption. However, the moderate refractive index of Si_3N_4 poses a challenge for efficient fiber-to-chip coupling using grating couplers. Although advantageous for wafer-scale testing and flexible layouts, Si_3N_4 grating couplers suffer from low grating strength, which limits their coupling efficiency. Here, we experimentally demonstrate high-efficiency grating couplers on a hybrid amorphous-silicon/silicon-nitride (a-Si/Si_3N_4) platform. Uniform devices are presented for TE and TM polarizations in both the O- and C-bands, while apodized-focalizing designs are demonstrated for both polarizations in the O-band and for TE polarization in the C-band. The fabricated devices achieved record coupling efficiencies of -1.6 dB and -1.2 dB in the O-band for TE and TM polarizations, respectively, and -1.3 dB and -2.9 dB in the C-band for TE and TM polarizations, respectively. The measured peak wavelengths deviated from their nominal values, primarily because of variations in the refractive index of the fabricated Si_3N_4 and the grating duty cycles relative to their design values. These shifts are well reproduced by simulations incorporating fabrication biases and can be compensated for by adjusting grating parameters or the fiber coupling angle. To the best of our knowledge, these are the highest coupling efficiencies demonstrated to date for silicon nitride grating couplers in the O-band for both polarizations and in the C-band for TM polarization. For TE polarization in the C-band, fabrication deviations shifted the peak coupling wavelength to 1512 nm, resulting in the highest efficiency reported to date for a silicon nitride grating coupler operating in the S-band. These results demonstrate a practical approach for achieving low-loss fiber-to-chip coupling in Si_3N_4 photonic integrated circuits, addressing a longstanding challenge in the platform and supporting the development of scalable systems for datacom, telecom, nonlinear photonics, and quantum technologies.

1. INTRODUCTION

The growing demand for high-capacity, energy-efficient systems has driven the photonics industry to diversify by leveraging the unique characteristics of different material platforms according to the requirements of specific applications. In particular, the silicon nitride (Si_3N_4) photonic integrated platform is now recognized as an important alternative to the currently predominant silicon-on-insulator (SOI) platform [1, 2]. With its lower refractive index, $n_{Si_3N_4} \approx 2$ [3], Si_3N_4 waveguides offer sufficient optical confinement while significantly reducing scattering losses from sidewall roughness relative to SOI [4, 5]. The lower refractive index contrast also relaxes sensitivity to fabrication deviations, enabling more consistent device performance [5–9]. The bandgap can range from 2.7 eV to 5.0 eV, corresponding to a transparency window that can extend down to wavelengths near 250 nm [4, 10]. These properties have positioned Si_3N_4 as an ideal candidate for applications in the visible spectrum, where SOI waveguides cannot be used [7, 11]. Furthermore, Si_3N_4 has a thermo-optic coefficient approximately one order of magnitude lower than that of silicon [3, 12], making it particularly robust to environmental fluctuations [13, 14]. Lastly, Si_3N_4 exhibits negligible two-photon absorption and is well suited for high-power and nonlinear photonics applications [15, 16].

Despite its numerous advantages, key challenges remain before the full potential of the Si_3N_4 platform can be realized. In particular, the development of high-efficiency fiber-to-chip coupling interfaces, which are essential for complex optical systems, is hindered by the moderate refractive index contrast between the Si_3N_4 core and silicon dioxide (SiO_2) cladding. Grating couplers [17–19], often favored over edge couplers because of their compatibility with flexible chip layouts and wafer-scale testing [20, 21], typically suffer from low grating strength in silicon nitride. Compared with SOI couplers, considerably less light is diffracted out of the chip over a propagation distance comparable to the mode-field diameter (MFD) of the optical fiber's Gaussian-like mode profile. As a result, the coupling loss of Si_3N_4 single-etch grating couplers has gener-

* Corresponding author: Pavel Cheben (pavel.cheben@nrc-cnrc.gc.ca).

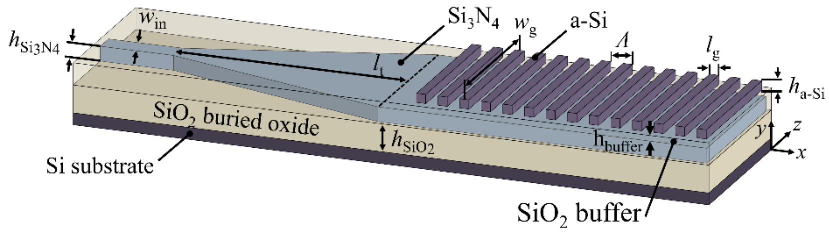

FIGURE 1. Schematic of a grating coupler based on the a-Si/Si_3N_4 platform with a silicon nitride waveguide layer and high-index amorphous silicon overlay grating.

ally been larger than -2 dB [22–27], whereas sub-1-dB coupling loss is readily achievable in SOI [28, 29].

Several strategies for enhancing the performance of Si_3N_4 grating couplers have been reported in the literature. Grating apodization provides some improvement by increasing the coupling efficiency (CE) via improved overlap between the optical fiber mode and the radiated field. However, apodization needs to be used in combination with other strategies that compensate for the low grating strength and directionality [30, 31]. Backside mirrors are a common approach for improving grating directionality by reflecting light toward the optical fiber that would otherwise be radiated into the substrate. This has been demonstrated with metallic mirrors [7, 31] or Bragg reflectors formed with alternating layers of silicon dioxide and silicon [32–35] or Si_3N_4 [36, 37]. Although this approach has yielded coupling efficiencies as high as -0.55 dB in the C-band [31], it requires specialized fabrication processes that make backside mirrors an inconvenient choice in many contexts where grating couplers are critical, such as wafer-scale testing in photonics manufacturing or rapid device prototyping.

Blazed gratings formed by angled or multi-level etching can similarly enhance directionality by promoting constructive interference in the upward direction [30, 38–40]. However, multiple etch depths are not commonly available on the Si_3N_4 platform. Instead, multi-layer configurations offer a practical solution, as the dual integration of silicon and Si_3N_4 layers is becoming increasingly common [41, 42]. Early demonstrations of this approach included Si_3N_4-on-SOI [43–45], dual-layer Si_3N_4 [46], and dual-layer Si_3N_4 on SOI [47]. More recently, depositing amorphous silicon (a-Si) on top of Si_3N_4 waveguides has gained significant attention because it leverages the high refractive index contrast of silicon gratings while limiting overlayer processing to the localized areas where the couplers are formed [48–53]. In simulations, this approach has yielded coupling efficiencies as high as -0.39 dB in the C-band [52] and -0.83 dB in the O-band with the inclusion of an aluminum mirror [54]. However, experimental demonstrations of a-Si/Si_3N_4 grating couplers have been limited. This strategy was implemented on an ultra-low-loss 100 nm Si_3N_4 platform, with a reported coupling efficiency of -5 dB [53]. On the 800 nm platform, a-Si/Si_3N_4 devices reached -1.4 dB and -2.2 dB in the C-band with and without a backside mirror, respectively, as well as -2.3 dB for TM polarization and -3.0 dB for TE polarization in a polarization-insensitive design in the O-band [51]. We believe that the potential of this approach is yet to be fully explored, especially on the common 400 nm Si_3N_4 platform, and that it is a promising path toward achieving sub-dB grating coupling loss in Si_3N_4 waveguides.

In earlier work [50], we proposed a high-efficiency grating coupler design based on Si_3N_4 waveguides with an amorphous silicon overlayer. Metamaterial grating apodization and beam focalization were combined to optimize coupler performance. Here, we move beyond previous design and simulation studies to demonstrate the concept experimentally for the first time. We report devices optimized for the O-band (1260–1360 nm) and C-band (1530–1565 nm), which are key wavelength regions for telecommunications and datacenter interconnects. This work marks a significant advancement in developing practical, high-efficiency coupling interfaces for Si_3N_4 integrated photonics.

2. WAVEGUIDE PLATFORM AND UNIFORM GRATING COUPLER DESIGN

Fig. 1 shows a three-dimensional (3D) diagram of a uniform grating coupler on our hybrid a-Si/Si_3N_4 photonic integration platform. This platform leverages the advantages of Si_3N_4 and silicon simultaneously on a single chip. The 400-nm-thick Si_3N_4 layer ($h_{Si_3N_4}$), with a 3.25-μm buried oxide layer (h_{SiO_2}), provides the interconnecting waveguides, which benefit from the comparatively low propagation loss of this platform. Meanwhile, the diffraction gratings are formed in the 220-nm amorphous silicon overlayer ($h_{\text{a-Si}}$) to exploit the higher refractive index of a-Si, thereby achieving high grating strength. A 100-nm SiO_2 buffer layer (h_{buffer}) separates the Si_3N_4 and a-Si layers to protect the waveguides during the grating definition step.

The grating couplers were designed using Ansys Lumerical finite-difference time-domain (FDTD) simulation software [55]. First, uniform grating couplers were designed as reference benchmarks. These couplers are defined by their period, Λ, and the length of the grating teeth, l_g, as shown in Fig. 1. The ratio between Λ and l_g defines the duty cycle (DC), which is commonly used to parameterize the longitudinal structure of the grating, i.e., along the x-axis in Fig. 1. The width of uniform grating couplers, w_g, as labelled in Fig. 1, is set such that the width of the mode propagating in the waveguide matches the MFD of the optical fiber mode. A linear adiabatic taper of length l_t is used to gradually transition from the single-mode interconnecting waveguide to the width w_g of the Si_3N_4 slab underneath the a-Si grating. Alternatively, the taper length can be reduced by curving the grating structure along circular arcs, with the input waveguide positioned at the centre of curvature [56]. This approach was not used

TABLE 1. Nominal parameters and simulated coupling characteristics for the uniform a-Si/Si_3N_4 grating couplers.

λ_0 (nm)	Polarization	Λ (nm)	DC (%)	Coupling angle	Coupling efficiency (dB)
1310	TE	550	32	-31°	-1.33
	TM	660	56	-13°	-1.28
1550	TE	950	42	9°	-1.38
	TM	730	52	-23°	-2.01

in this work, as it could introduce increased sensitivity to misalignment between the Si_3N_4 and a-Si structures. For a uniform grating coupler, the diffraction angle θ is given by the grating equation [57]:

$$n_{\text{clad}} \sin\theta = n_{\mathit{eff}} + \frac{m\lambda}{\Lambda} \tag{1}$$

where n_{clad} is the refractive index of the top cladding; n_{eff} is the effective index of the Floquet-Bloch mode propagating in the grating region [58, 59]; m is the diffraction order; λ is the free-space wavelength; and Λ is the grating period.

In simulations, the coupling efficiency is calculated as the product of the power radiated upward by the grating (P_{up}) and the field overlap (OL) between the radiated field and the optical fiber mode profile. The couplers were designed for standard single-mode fibers, which have a near-Gaussian mode profile with mode-field diameters (MFDs) of 9.2 µm and 10.4 µm at the central wavelengths of the O-band (1310 nm) and C-band (1550 nm), respectively. The field overlap between the optical fiber mode E_f and the field radiated by the grating E_g was calculated using the complex overlap integral:

$$\text{OL} = \frac{\int \left| E_g E_f^* dA \right|^2}{\int \left| E_g E_g^* \right| dA \int \left| E_f E_f^* \right| dA} \tag{2}$$

Optimal parameters for uniform grating couplers were obtained by performing a sweep of the period and duty cycle using two-dimensional (2D) FDTD simulations of the device cross-section in the x-y plane. For each parameter set, the coupling efficiency was calculated and saved in a design map, which was then used to identify the best candidates. Optimized parameters and simulated coupling characteristics are summarized in Table 1.

The advantage provided by the high-index a-Si overlayer is clear from the predicted coupling efficiencies summarized in Table 1. Forming the grating structure above the Si_3N_4 waveguides breaks the vertical symmetry, which enhances the grating's directionality and therefore improves performance via a direct increase in P_{up}. Another important factor linked to directionality is the coupling angle. Reflection of the downward-radiated light at the interface between the SiO_2 and the Si substrate produces a Fabry-Perot effect. For each wavelength, there are specific diffraction angles at which the interference is constructive in the upward direction, toward the fiber, rather than downward into the substrate. Therefore, the angle is treated as a free parameter to achieve the highest coupling efficiency. The devices listed in Table 1 have different coupling angles chosen to minimize power lost through leakage into the substrate.

3. APODIZED-FOCALIZING GRATING COUPLER DESIGN

Next, we enhance the coupling performance via apodization and beam focalization. Uniform grating couplers have a constant grating strength, resulting in a radiated field with a decaying exponential profile whose overlap with a Gaussian profile is theoretically limited to 80% [18, 19, 60]. Apodization is used to vary the grating strength along the coupler length and thereby reshape the radiated field. A Gaussian beam can be produced by gradually increasing the grating strength at the beginning of the coupler, followed by uniform periods at the peak grating strength [61]. We apodized the structure using subwavelength metamaterials [62–64]. These periodic structures have a pitch significantly smaller than the wavelength, allowing them to form an effectively homogeneous anisotropic medium with an equivalent refractive index between those of constituent materials [65, 66]. This additional degree of freedom in refractive-index control has been used to enhance the performance of grating couplers on both SOI [67–70] and Si_3N_4 platforms [26, 27]. Here, we implement this approach for the first time on an a-Si-on-Si_3N_4 platform.

In our design, trenches with a subwavelength periodicity Λ_{swg} along the transverse axis are etched into the first few periods of the coupler to control the grating strength. The duty cycle of the subwavelength structure, which sets the segment width w_{swg}, is gradually increased along the grating to achieve apodization effect through the corresponding evolution of the refractive index contrast. Fig. 2 illustrates a 3D schematic of the apodized-focalizing (AF) grating coupler.

In an apodized grating coupler, the reduced grating strength in the first few periods translates to less upward-radiated power (P_{up}) than a uniform device of the same length operating at the highest grating strength. Although this improves field overlap and reduces back-reflections, the performance gains can be offset by reducing upward-radiated power. To mitigate this effect, we use beam focalization, leveraging a grating geometry that shapes the wavefront to focus the light into a fiber positioned at a specific height above the chip surface [27, 30, 31, 38, 50, 71]. Since the wavefront emitted by the grating converges toward the fiber, the field diameter near the chip surface is larger than that of the fiber mode. This relaxes the trade-off between overlap and P_{up}, since a longer structure can be used to compensate for the lower grating strength in the initial periods by radiating more light over a longer propagation distance. Along the

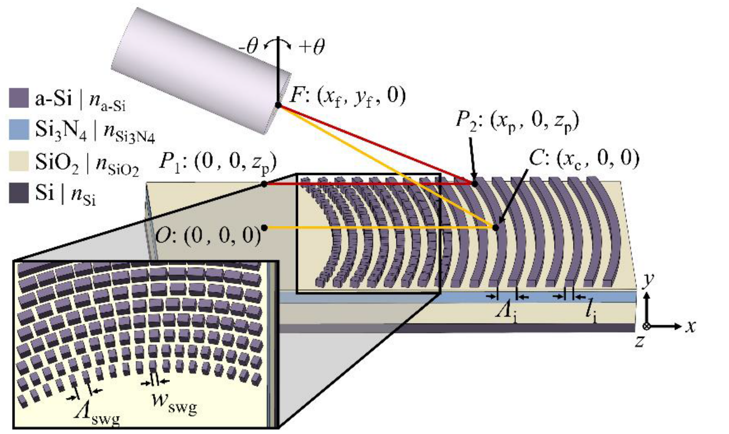

FIGURE 2. Grating coupler for Si_3N_4 waveguides with an a-Si overlayer, featuring subwavelength metamaterial apodization and beam focalization. The labelled coordinates were used to calculate the curvature of the grating structure.

TABLE 2. Optimized parameters of the apodized-focalizing grating couplers.

	O-band TE	O-band TM	C-band TE
Number of apodized periods	7	8	11
Number of homogeneous periods	41	29	37
Grating period (nm)	537–585	631–706	835–914
Metamaterial index	2.4 — $n_{a\text{-}Si}$	1.8 — $n_{a\text{-}Si}$	1.9 — $n_{a\text{-}Si}$
Diffraction angle	$-23° – -35°$	$-7° – -18°$	$-2°$–$6°$
Duty cycle	26%	40%	28%
Optical fibre height	55 μm	55 μm	75 μm
Optical fibre angle	$-26°$	$-7°$	$4°$
Simulated coupling efficiency	-0.91 dB	-1.17 dB	-1.03 dB

longitudinal axis, focalization is achieved by chirping the period to gradually vary the diffraction angle from an initial angle θ_i to a final angle θ_f, in accordance with Eq. (1), as the light propagates through the grating. Focalization along the transverse axis is implemented by curving the grating structure, as illustrated in Fig. 2.

The coupler's longitudinal geometry is defined by the number of periods in the metamaterial-apodized section (N_{apo}) and in the uniform section (N_u), metamaterial refractive indices (n_{swg}), structural parameters of unetched grating teeth (Λ_i and l_i), and grating curvature. These parameters were optimized using a genetic algorithm (GA) based on 2D simulations of the coupler's longitudinal cross-section. In these simulations, the metamaterial is represented as a homogeneous medium with refractive index n_{swg}. Once n_{swg} values are optimized, Λ_{swg} and w_{swg} parameters required to synthesize these metamaterial indices are determined. At each iteration of the GA optimization, the algorithm selects values for N_{apo} and N_u, the initial and final grating strengths in the apodized section, and the radiation angles θ_i and θ_f. These values are then mapped to corresponding metamaterial indices and structural parameters according to characteristics selected by the GA. To simplify the design process, the grating duty cycle (l_i/Λ_i) is kept constant throughout the coupler, so that only the appropriate Λ_i needs to be selected. The coupling efficiency, calculated from a 2D simulation, is then used to update the parameters in the optimization algorithm. This iterative process continues until the algorithm converges to a design with optimal performance. Parameterizing the grating geometry and using computationally efficient 2D simulations accelerate convergence of the GA process. As shown in [50], an optimized design can be obtained after a few thousand simulations. Because each 2D simulation requires only a few seconds, the entire optimization can typically be completed in several hours. To further refine the design, the optimization was repeated for different fiber heights. There is a trade-off between focal length and bandwidth due to the dispersive nature of the beam-focalization phase profile [71]. Optimal fiber height was chosen to be as short as possible to maximize the bandwidth while maintaining high coupling efficiency.

Table 2 summarizes optimized parameters and 2D simulation results of apodized-focalizing grating couplers. For the TE polarization in the O-band, the equivalent metamaterial refractive index is increased from 2.4 to $n_{\text{a-Si}} = 3.9376$ (at 1310 nm) over the first 7 periods of the grating. The duty cycle is 26%, and the grating period is chirped from 585 nm to 577 nm in the apodized section and then from 575 nm to 537 nm in the following 41 periods with homogeneous grating strength. This results in a diffraction-angle change from $-23°$ to $-35°$ along the propagation direction over the full length of the coupler. The phase-chirping effect focalizes the diffracted beam field along

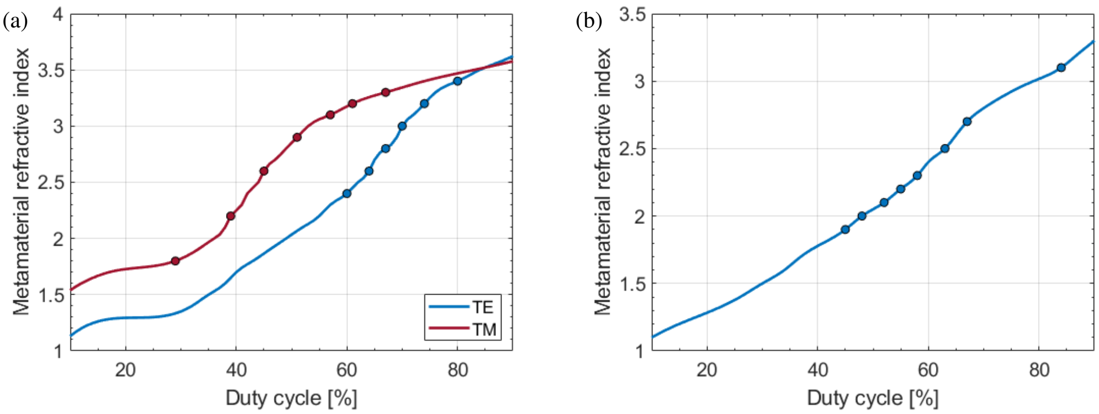

FIGURE 3. Model of the equivalent metamaterial refractive index as a function of the duty cycle with $\Lambda_{\text{swg}} = 600\,\text{nm}$ in the (a) O-band and (b) C-band for TE polarization. The highlighted points indicate the parameters used to synthesize the n_{swg} values obtained from the GA optimization.

the longitudinal direction to the target mode size of 9.2 µm at a focal distance of 55 µm above the chip surface. The total coupler length is 26.8 µm, and the 2D simulations predict a fiber-to-chip coupling efficiency of -0.91 dB with the fiber positioned at an angle of $-26°$. The high efficiency is obtained primarily because of the high directionality of 91%, the mode-field overlap of 92%, and very low back-reflections of 0.02% (-37 dB).

The GA-optimized design for the TM polarization in the O-band has metamaterials with equivalent refractive indices ranging from 1.8 to $n_{\text{a-Si}}$ over 8 periods of the apodized section. The grating has a uniform duty cycle of 40%, and the period is chirped from 706 nm to 697 nm in the apodized section and from 697 nm to 631 nm in the remaining 29 periods, resulting in a total length of 24.9 µm. Light is coupled to a fiber 55 µm above the chip at an angle of $-7°$. The calculated directionality is 88%, the overlap integral is 92%, and the back-reflections are 1% (-20 dB). The coupling efficiency in 2D FDTD simulations was -1.17 dB, with a 1-dB bandwidth of 28 nm.

For the TE polarization in the C-band, the SWG equivalent refractive index in the optimized design varies from 1.9 to $n_{\text{a-Si}} = 3.8287$ (at 1550 nm) over the first 11 periods of the grating. In the apodized section, the grating period is chirped from 914 nm to 885 nm. The homogeneous section comprises 37 periods with a pitch ranging from 884 nm to 835 nm. The grating's duty cycle is 28%. Light is coupled to a fiber 75 µm above the chip at an angle of 4°. The total coupler length is 41.7 µm, and the directionality is 84%. The calculated overlap integral reaches 95%, while the back-reflections are 0.56% (-22 dB). The 2D FDTD simulations predict a coupling efficiency of -1.03 dB and a 1-dB bandwidth of 28 nm.

Apodization provided only a minimal performance increase for the TM polarization in the C-band compared with the other devices. Therefore, only the uniform device was developed for this case, allowing chip space to be prioritized for the higher-efficiency O-band and TE-polarized C-band designs. After the 2D optimization was completed, the final design step was to determine the structural parameters of the metamaterials and the transverse geometry of the coupler. Based on minimum feature sizes achievable with the fabrication process, an SWG pitch of $\Lambda_{\text{swg}} = 600\,\text{nm}$ was used to accommodate the wide range of equivalent metamaterial refractive indices in our optimized designs. Although this pitch is larger than what would be generally considered the deep-subwavelength regime, where analytical models provide accurate parameter fits [62, 63, 69], 3D FDTD simulations showed that it is sufficiently small to suppress diffraction effects. A model describing the relationship between the duty cycle of the subwavelength structures ($w_{\text{swg}}/\Lambda_{\text{swg}}$) and their equivalent refractive index in our a-Si/Si_3N_4 configuration was created using two sets of 3D FDTD simulations. First, using parameters in Table 1, uniform grating couplers were simulated with grating teeth replaced by a material with a manually defined refractive index. The index was swept from 1 to $n_{\text{a-Si}}$ to capture the dependence of grating strength on the refractive index of the grating teeth. The grating teeth material was then reset to a-Si, and the teeth were segmented along the transverse axis to form the subwavelength metamaterial with $\Lambda_{\text{swg}} = 600\,\text{nm}$. A second simulation sweep was performed, varying the duty cycle of subwavelength structures from 0% to 100% in steps of 1%. The relationship between duty cycle and equivalent refractive index was then determined by comparing the grating strengths and diffraction angles from the two 3D FDTD simulation sweeps. The parameter fit with the selected metamaterial parameters is plotted for the O-band in Fig. 3(a) and for the TE polarization in the C-band in Fig. 3(b).

We employ a ray-optics approach to design the grating curvature that provides beam focalization along the transverse axis of the grating coupler. For each period of grating, the tooth is curved such that the optical path length between any point on the plane phase front entering the coupler and the optical fiber is constant along a given grating tooth. This is done by solving Eq. (3) using the coordinates labelled in Fig. 2 and the effective index, n_{eff}:

$$\begin{aligned} & n_{\mathit{eff}}\, x_p + \sqrt{\left(x_p - x_f\right)^2 + y_f^2 + z_p^2} \\ = \; & n_{\mathit{eff}}\, x_c + \sqrt{\left(x_c - x_f\right)^2 + y_f^2} \end{aligned} \tag{3}$$

Since the longitudinal structure of the grating was determined during the 2D optimization process, the central point of each

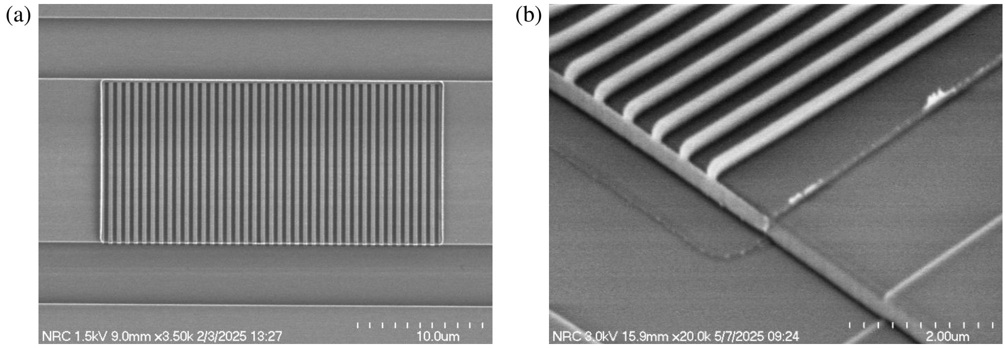

FIGURE 4. Scanning electron microscope images of uniform a-Si/Si_3N_4 grating couplers, showing (a) top and (b) angled views.

grating tooth, labelled as point C in Fig. 2, was used as a reference to simplify the calculation of remaining coordinates.

4. FABRICATION AND EXPERIMENTAL RESULTS

We used a 200 mm silicon wafer with a 3.25 µm SiO_2 buried oxide and a 400 nm Si_3N_4 layer formed by a low-pressure chemical vapour deposition (LPCVD) process. The waveguide patterns were defined using 248 nm deep ultraviolet (DUV) lithography with a 680 nm-thick JSR M91Y positive-tone resist, followed by inductively coupled plasma (ICP) etching using SF_6/C_4F_8 chemistry. The resist was removed using O_2 plasma and an RCA-1 cleaning step. Afterwards, the 100 nm SiO_2 buffer layer was deposited using plasma-enhanced chemical vapour deposition (PECVD). This was followed by a second DUV lithography step with a 1.3 µm M91Y resist to define the overall region enclosing the grating coupler, onto which 220 nm of amorphous silicon was sputtered and patterned by lift-off. The wafer was then diced into individual chips for sample-level processing. Each sample was spin-coated with a 250 nm ZEP resist, and the grating patterns were defined using electron-beam lithography. These patterns were transferred into the a-Si layer using ICP etching, with slight over-etching ($\sim$10 nm) into the buffer oxide. The final resist removal was performed using an N-Methyl-2-pyrrolidone cleaning process.

Several design variations were fabricated in addition to nominal designs to compensate for fabrication uncertainties, such as changes in layer thickness, deviations in the refractive indices of a-Si or Si_3N_4, and over- or under-etching of the grating structures. For the uniform couplers, these variations included biases of $\pm$20 nm in the grating period and $\pm$5% in the duty cycle. For apodized-focalizing couplers, the variations covered a range of $\pm$5% for the duty cycles of both the diffraction grating and the subwavelength grating, as well as variations in the grating radii of curvature.

4.1. Uniform Grating Coupler

Fig. 4 shows scanning electron microscope (SEM) images of uniform grating couplers on the a-Si/Si_3N_4 platform. The devices were characterized in a back-to-back configuration using fiber-chip-fiber transmission measurements. For the O-band test structures, the single-mode interconnecting waveguides have a width of 0.8 µm, with a total length of 3.05 mm. The couplers have a width of 13.1 µm and are connected to the single-mode input waveguide by a 180-µm-long linear taper. In the C-band, the input waveguide width is 1 µm, and the propagation distance between couplers is 2.55 mm. The tapers have a length of 180 µm for a grating width of 15 µm.

Separate test structures were fabricated to measure waveguide propagation losses using the cut-back method. Based on these measurements, the waveguide loss was determined to be 0.72 dB/cm (TE) and 0.78 dB/cm (TM) in the O-band, and 1.14 dB/cm (TE) and 1.18 dB/cm (TM) in the C-band. Fiber-to-fiber transmission measurements without the chips were performed to determine the setup loss, which includes the loss of the fiber patch cords and the polarization controller. The loss of linear tapers was considered to be part of the coupler loss. Based on 3D FDTD simulations, the taper loss is expected to be below 0.2 dB. The waveguide loss ($l_{\text{wg}}\alpha_{\text{wg}}$) and the experimental-setup loss (α_{sys}) were subtracted from the measured back-to-back transmittance (T) to obtain the coupler's efficiency CE using Eq. (4). We note that factor 2 in the denominator accounts for the two nominally identical grating couplers in each back-to-back test structure.

$$\text{CE} = \frac{T - l_{\text{wg}}\alpha_{\text{wg}} - \alpha_{\text{sys}}}{2} \tag{4}$$

Beginning with O-band designs, the fabricated uniform grating coupler with the best performance for TE polarization was the variation with a grating period of 570 nm and a duty cycle of 37%. Fig. 5(a) plots the measured coupling efficiency. The measured peak coupling efficiency was -2.2 dB, with a 1-dB bandwidth of 31 nm centred at 1308 nm. The simulation result for a uniform grating coupler with the same parameters is shown by the red curve. These results show the influence of deviations between nominal design parameters and fabricated devices. The structural and material parameters of the simulation model were varied in a series of FDTD simulations, and the calculated coupling efficiency was compared with the experimental results. It was found that reductions in the refractive index of the Si_3N_4 layer and in the grating duty cycle yielded a more accurate model of the fabricated devices. Such fabrication deviations are reasonable considering the potential variability of the refractive index during the formation of Si_3N_4 films [4, 10] and fabrication errors during the patterning step of the a-Si gratings.

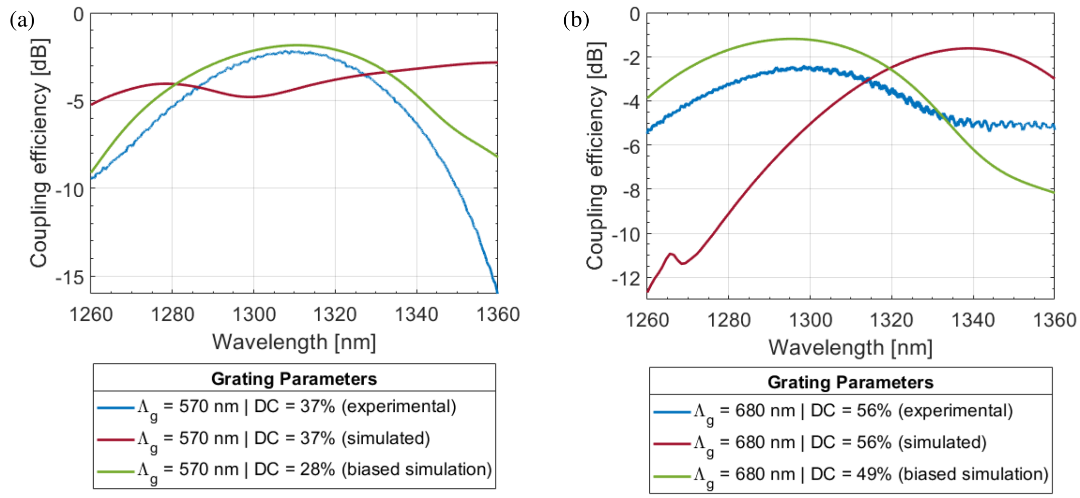

FIGURE 5. Experimental results showing the highest coupling efficiencies achieved with uniform a-Si/Si_3N_4 grating couplers designed for (a) TE and (b) TM polarizations in the O-band.

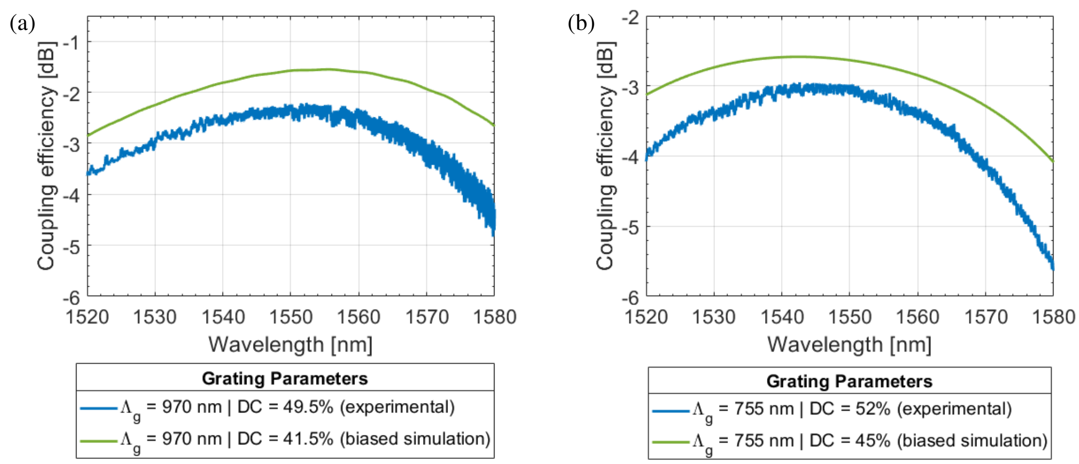

FIGURE 6. Experimental results showing the highest coupling efficiencies achieved with uniform a-Si/Si_3N_4 grating couplers designed for (a) TE and (b) TM polarizations in the C-band.

The best agreement with experimental results for TE polarization in the O-band was found with a 3% reduction in the Si_3N_4 refractive index ($n_{Si_3N_4} = 2.0654$ at 1310 nm) and a 9% reduction in the grating duty cycle. The corresponding simulated coupling efficiency is shown in Fig. 5(a) (green curve). For TM polarization, a peak coupling efficiency of -2.4 dB, with a 1-dB bandwidth of 39 nm centred at 1300 nm, was achieved by the coupler with a nominal period of 680 nm and a duty cycle of 56%. Fig. 5(b) plots experimental and simulated results. Following the analysis for TE polarization, it was determined that the fabricated device had a coupling efficiency consistent with the same 3% reduction in Si_3N_4 refractive index and a grating duty cycle reduced to 49% (Fig. 5(b), green curve).

For TE polarization in the C-band, a peak coupling efficiency of -2.2 dB was measured for the grating with a period of 970 nm and a duty cycle of 49.5%. The corresponding 1-dB bandwidth was 47 nm. Fig. 6(a) shows experimental results (blue curve) and biased simulation results (green curve) with the best agreement. The difference between the simulated and measured coupling efficiencies is consistent with the trend observed for the O-band devices. Introducing a bias in the silicon nitride refractive index ($n_{Si_3N_4} = 2.0631$ at 1550 nm) and including an over-etch of the grating trenches in the FDTD model yielded the best alignment of the peak wavelength between the simulated coupling efficiency and the experimental measurement. The duty cycle in the biased simulation was reduced to 41.5%.

Next, a peak coupling efficiency of -2.9 dB, with a 1-dB bandwidth of 48 nm, was measured for TM polarization. The best performance grating had a period of 755 nm and a duty cycle of 52%. Fig. 6(b) plots the coupling efficiency of the fabricated device with the corresponding simulation results. In the biased simulations with a lower Si_3N_4 refractive index, a duty cycle of 45% compensated for the shift between the experimental and simulated peak coupling wavelengths.

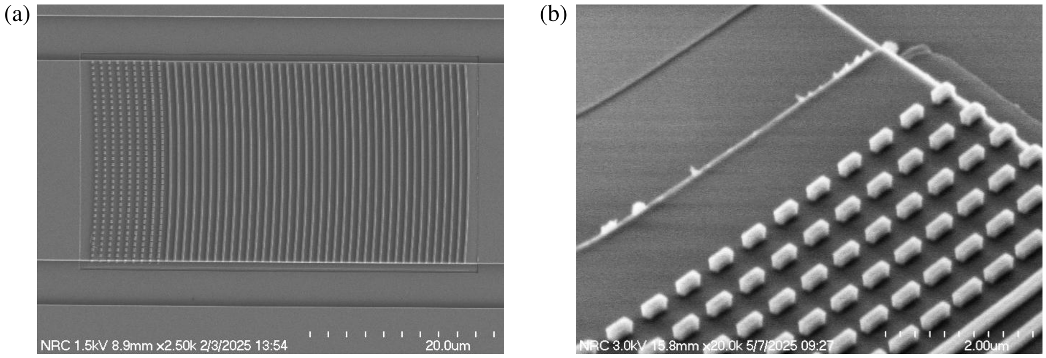

FIGURE 7. SEM images showing (a) top and (b) angled views of an apodized-focalizing a-Si/Si_3N_4 grating coupler with subwavelength metamaterials.

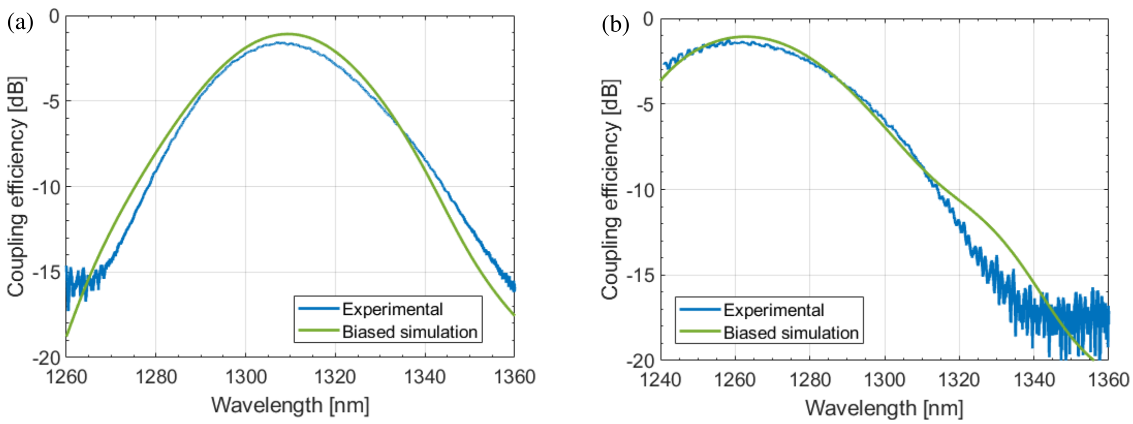

FIGURE 8. Coupling-efficiency spectra for apodized-focalizing a-Si/Si_3N_4 grating couplers designed for (a) TE and (b) TM polarizations in the O-band, showing experimental results (blue curves) and simulation results for the corresponding biased devices (green curves).

Overall, the performance of uniform a-Si/Si_3N_4 grating couplers represents a modest improvement over single-etch Si_3N_4-only grating couplers [26, 27] and is comparable to previously reported mirrorless multi-layer approaches [51].

4.2. Apodized-Focalizing Grating Coupler

Finally, we present experimental results for apodized-focalizing devices. By implementing subwavelength metamaterial apodization and wavefront focusing on the a-Si/Si_3N_4 platform, we bring the experimental performance close to the 1-dB level.

Fig. 7 shows scanning electron microscope images of one of the fabricated apodized-focalizing grating couplers. For the O-band test structures, the single-mode interconnecting waveguides have a width of 0.8 μm and a total length of 2.60 mm. The taper length is 450 μm, and the grating has a width of 19.1 μm. In the C-band, the input waveguide width is 1 μm, and the propagation distance between couplers is 1.26 mm. The tapers have a length of 600 μm for a grating width of 21.8 μm.

The couplers were characterized using the same back-to-back methodology as uniform devices. An initial measurement of the coupling efficiency was taken with the fibers positioned close to the chip surface. The fibers were then raised incrementally, with additional transmission measurements taken at each subsequent height. This process was repeated for every fabricated device variation to identify the coupler with the best performance.

For TE polarization in the O-band, a maximum coupling efficiency of -1.6 dB was achieved by the device with a 5% fabrication bias applied to the grating duty cycle. Fig. 8(a) shows experimental results. The 1-dB bandwidth was measured to be 20 nm, centred at a wavelength of 1307 nm. This trade-off between peak coupling efficiency and optical bandwidth, compared with uniform devices, is due to the wavelength-dependent beam-focalizing phase profile. Initial measurements taken at the nominal angle of $-26°$ exhibited a peak efficiency shifted toward the lower end of the O-band. This shift was corrected by increasing the fiber angle to $-32°$.

As with uniform devices, the performance of fabricated apodized-focalizing couplers differs from simulation results. The green line in Fig. 8(a) shows the simulation results with the duty cycle reduced by 4% and using the corrected value of the Si_3N_4 refractive index. This fabrication bias is consistent with the observations from the uniform devices and produces simulations that more accurately model the fabricated devices. For TM polarization, the nominal design variant yielded a peak coupling efficiency of -1.2 dB with a 1-dB bandwidth of 32 nm. As shown by experimental results in Fig. 8(b), the peak wavelength was shifted toward shorter wavelengths, with the peak

TABLE 3. High-efficiency Si_3N_4-based grating couplers with multilayer configurations or backside reflectors.

Wavelength	Polarization	Description	Peak CE (dB)	1-dB bandwidth (nm)	Reference
	TE	Dual-layer grating	−2.2	72.9	[6]
	TE/TM	Tri-layer grating	−4.8	100	[7]
	TE/TM	Overlay grating	−2.2	–	[8]
O-band	TE	Overlay grating	−2.2	31	
	TE	AF overlay grating	−1.6	20	This work
	TM	Overlay grating	−2.4	39	
	TM	AF overlay grating	−1.2	32	
	TE	Overlay grating	−2.2	45	[8]
	TE	Overlay and metallic reflector	−1.4	37.5	[8]
	TE	Bragg reflector	−1.17	40	[9]
C-band	TE	AF with metallic reflector	−0.55	–	[10]
	TE	Dual-layer grating	−1.3	80	[11]
	TE	Overlay grating	−2.2	47	
	TE (S-band)	AF overlay grating	−1.3	24	This work
	TM	Overlay grating	−2.9	48	

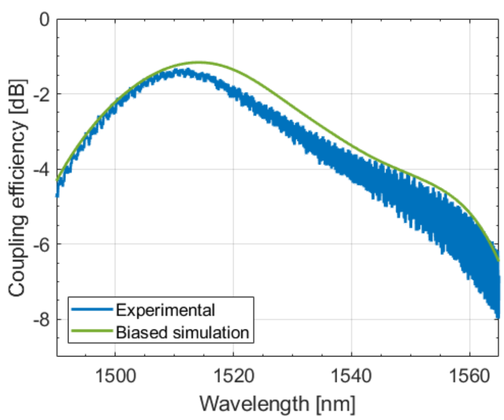

FIGURE 9. Experimental coupling efficiency and corresponding biased simulation results for the apodized-focalizing a-Si/Si_3N_4 grating coupler designed for TE polarization in the C-band.

coupling efficiency occurring at 1260 nm. In this case, increasing the fiber angle to compensate for the wavelength shift resulted in a deterioration of the peak coupling efficiency.

A peak coupling efficiency of −1.3 dB was achieved for TE polarization by the coupler with a 5% bias applied to the diffraction-grating duty cycle and a 2.5% bias applied to the subwavelength-grating duty cycle. Fig. 9 shows experimental results and corresponding biased simulation results. As for the O-band couplers, the peak coupling efficiency is blue-shifted. The 1-dB bandwidth is 24 nm, centred at 1512 nm. Furthermore, since this design operates at a positive diffraction angle, the fiber angle would have to be reduced to compensate for the wavelength shift. However, due to physical limitations of the fiber mount used in the experimental testing station, the angle could not be reduced below 5°. Although the wavelength of 1512 nm is outside the C-band, it falls within the S-band, which has gained significant interest for multi-band fiber communication networks [72].

5. SUMMARY AND CONCLUSION

For all three design cases, apodized-focalizing grating couplers yielded a substantial improvement over uniform devices. In the O-band, the peak coupling efficiency was increased by 0.6 dB and 1.2 dB for TE and TM polarizations, respectively. Similarly, a 0.9 dB performance enhancement was achieved for TE polarization in the C-band. The wavelength shifts in the peak coupling efficiency observed for TM polarization in the O-band and TE polarization in the C-band can be readily corrected by adjusting the grating period, as was done with uniform devices. In Table 3, our results are compared with previously reported experimental demonstrations of high-efficiency Si_3N_4-based grating couplers using non-standard fabrication approaches based on backside reflectors and multilayer stacks.

To the best of our knowledge, peak coupling efficiencies of −1.6 dB and −1.2 dB for TE and TM polarizations, respectively, are the highest reported to date in the O-band on a Si_3N_4 platform. With the addition of a metallic backside mirror, our FDTD simulations predict that the performance could be further enhanced to −0.5 dB for TE polarization and −0.7 dB for TM polarization. Furthermore, we have demonstrated excellent performance in the C-band. For TE polarization, our result of −1.3 dB represents the highest efficiency reported to date without using metallic or Bragg reflectors, which would require custom backside processing steps. The grating is also etched on a single layer, making it more fabrication-robust compared to multi-layer geometries. While comparable performance has been reported for a Si_3N_4-on-SOI configuration [43], that approach requires gratings formed in both layers of the chip, which increases the sensitivity to layer misalignment. Lastly, our uniform design with a coupling efficiency of −2.9 dB marks a 3.6 dB improvement over previously reported Si_3N_4 devices for TM polarization in the C-band [73].

In this work, we have presented the design and experimental demonstration of high-efficiency grating couplers for Si_3N_4

waveguides using an amorphous silicon overlayer. Forming the grating structure in a higher-index top layer breaks the device's vertical symmetry, enabling higher grating strength and improved directionality compared with moderate-index-contrast Si_3N_4 gratings. Although this hybrid a-Si/Si_3N_4 platform adds some complexity to the fabrication process, the overlayer processing is confined to the small grating-coupler region. The packaging tolerance is governed by the coupler's alignment tolerance, which is comparable to that of conventional grating couplers. Furthermore, for large-scale manufacturing, the electron-beam lithography used here to define the grating can be replaced with DUV lithography. Both uniform and apodized-focalizing devices were developed. In the O-band, the uniform couplers yielded superior performance compared with Si_3N_4-only devices and matched the results of advanced multilayer designs reported in the literature. We achieved record coupling efficiencies in this wavelength region of -1.6 dB and -1.2 dB by combining subwavelength grating apodization and beam focalization with genetic-algorithm optimization. In the C-band, the uniform coupler yielded a coupling efficiency of -2.9 dB, the highest reported to date for TM polarization. Lastly, the coupling efficiency of -1.3 dB achieved with the apodized focalizing design for TE polarization would represent record performance for a Si_3N_4 coupler designed for the C-band without a backside reflector or multilayer etched-grating patterns. However, due to fabrication deviations and the physical limitations of our experimental setup, this coupling efficiency was measured at 1512 nm, making it the best performance demonstrated to date for a silicon nitride grating coupler in the S-band. These results reinforce the effectiveness of our grating-coupler design methodology on the hybrid a-Si/Si_3N_4 platform. By combining high efficiency, broadband performance, and compatibility with standard fabrication processes, this work addresses one of the key challenges in Si_3N_4 photonics. The demonstrated hybrid a-Si/Si_3N_4 platform offers a practical solution for reducing coupling losses while supporting wafer-scale fabrication and testing. Combined with subwavelength metamaterial apodization and advanced optimization techniques, this approach offers new opportunities to address additional fiber-chip coupling challenges, such as polarization diversity and multiband operation using two-dimensional gratings. As Si_3N_4 photonic circuits continue to grow in complexity and functionality, these advances will help enable high-performance systems for optical communications, sensing, microwave photonics, and quantum applications.

ACKNOWLEDGEMENT

This work was supported in part by the National Research Council of Canada under Grant CSTIP STR-20104, in part by the Natural Sciences and Engineering Research Council of Canada (NSERC) Discovery Grant, in part by the EU NextGenerationEU Recovery and Resilience Plan for Slovakia under Project 9I03-03-V04-00410, and in part by the UK EPSRC grant juNIPeRS (EP/T007303/1).

REFERENCES

[1] Blumenthal, D. J., R. Heideman, D. Geuzebroek, A. Leinse, and C. Roeloffzen, "Silicon nitride in silicon photonics," *Proceedings of the IEEE*, Vol. 106, No. 12, 2209–2231, Dec. 2018.

[2] Siew, S. Y., B. Li, F. Gao, H. Y. Zheng, W. Zhang, P. Guo, *et al.*, "Review of silicon photonics technology and platform development," *Journal of Lightwave Technology*, Vol. 39, No. 13, 4374–4389, Jul. 2021.

[3] Arbabi, A. and L. L. Goddard, "Measurements of the refractive indices and thermo-optic coefficients of Si_3N_4 and SiOx using microring resonances," *Optics Letters*, Vol. 38, No. 19, 3878–3881, 2013.

[4] Gardes, F., A. Shooa, G. De Paoli, I. Skandalos, S. Ilie, T. Rutirawut, W. Talataisong, J. Faneca, V. Vitali, Y. Hou, *et al.*, "A review of capabilities and scope for hybrid integration offered by silicon-nitride-based photonic integrated circuits," *Sensors*, Vol. 22, No. 11, 4227, Jun. 2022.

[5] Wilmart, Q., H. El Dirani, N. Tyler, D. Fowler, S. Malhouitre, S. Garcia, *et al.*, "A versatile silicon-silicon nitride photonics platform for enhanced functionalities and applications," *Applied Sciences*, Vol. 9, No. 2, 255, Jan. 2019.

[6] Baets, R., A. Z. Subramanian, S. Clemmen, B. Kuyken, P. Bienstman, N. Le Thomas, G. Roelkens, D. Van Thourhout, P. Helin, and S. Severi, "Silicon photonics: Silicon nitride versus silicon-on-insulator," in *Optical Fiber Communication Conference*, Th3J.1, Anaheim, California, 2016.

[7] Romero-García, S., F. Merget, F. Zhong, H. Finkelstein, and J. Witzens, "Silicon nitride CMOS-compatible platform for integrated photonics applications at visible wavelengths," *Optics Express*, Vol. 21, No. 12, 14 036–14 046, Jun. 2013.

[8] Tan, D. T. H., D. K. T. Ng, J. W. Choi, E. Sahin, B. U. Sohn, G. F. R. Chen, P. Xing, H. Gao, and Y. Cao, "Nonlinear optics in ultra-silicon-rich nitride devices: Recent developments and future outlook," *Advances in Physics: X*, Vol. 6, No. 1, 1905544, 2021.

[9] Vitali, V., T. D. Bucio, H. Liu, J. M. L. González, *et al.*, "Fully integrated and broadband Si-rich silicon nitride wavelength converter based on Bragg scattering intermodal four-wave mixing," *Photonics Research*, Vol. 12, No. 3, A1, 2024.

[10] Bucio, T. D., C. Lacava, M. Clementi, J. Faneca, I. Skandalos, A. Baldycheva, *et al.*, "Silicon nitride photonics for the near-infrared," *IEEE Journal of Selected Topics in Quantum Electronics*, Vol. 26, No. 2, 1–13, Mar.–Apr. 2020.

[11] Smith, J. A., H. Francis, G. Navickaite, and M. J. Strain, "SiN foundry platform for high performance visible light integrated photonics," *Optical Materials Express*, Vol. 13, No. 2, 458–468, 2023.

[12] Wörhoff, K., R. G. Heideman, A. Leinse, and M. Hoekman, "TriPleX: A versatile dielectric photonic platform," *Advanced Optical Technologies*, Vol. 4, No. 2, 189–207, 2015.

[13] Gao, G., D. Chen, S. Tao, Y. Zhang, S. Zhu, X. Xiao, and J. Xia, "Silicon nitride O-band (de)multiplexers with low thermal sensitivity," *Optics Express*, Vol. 25, No. 11, 12 260–12 267, May 2017.

[14] Bucio, T. D., A. Z. Khokhar, G. Mashanovich, and F. Y. Gardes, "Athermal silicon nitride angled MMI wavelength division (de)multiplexers for the near-infrared," *Optics Express*, Vol. 25, No. 22, 27 310–27 320, Oct. 2017.

[15] Moss, D. J., R. Morandotti, A. L. Gaeta, and M. Lipson, "New CMOS-compatible platforms based on silicon nitride and Hydex for nonlinear optics," *Nature Photonics*, Vol. 7, No. 8, 597–607, 2013.

[16] Pfeiffer, M., A. Kordts, V. Brasch, M. Zervas, M. Geiselmann, J. Jost, and T. Kippenberg, "Photonic Damascene process for integrated high-Q microresonator based nonlinear photonics," *Optica*, Vol. 3, No. 1, 20–25, Jan. 2016.

[17] Tamir, T. and S.-T. Peng, "Analysis and design of grating couplers," *Applied Physics*, Vol. 14, No. 3, 235–254, Nov. 1977.

[18] Waldhäusl, R., B. Schnabel, P. Dannberg, E.-B. Kley, A. Bräuer, and W. Karthe, "Efficient coupling into polymer waveguides by gratings," *Applied Optics*, Vol. 36, No. 36, 9383–9390, Dec. 1997.

[19] Taillaert, D., F. Van Laere, M. Ayre, W. Bogaerts, D. Van Thourhout, P. Bienstman, and R. Baets, "Grating couplers for coupling between optical fibers and nanophotonic waveguides," *Japanese Journal of Applied Physics*, Vol. 45, No. 8R, 6071, 2006.

[20] Marchetti, R., C. Lacava, L. Carroll, K. Gradkowski, and P. Minzioni, "Coupling strategies for silicon photonics integrated chips [Invited]," *Photonics Research*, Vol. 7, No. 2, 201–239, 2019.

[21] Vermeulen, D. and C. V. Poulton, "Optical interfaces for silicon photonic circuits," *Proceedings of the IEEE*, Vol. 106, No. 12, 2270–2280, Dec. 2018.

[22] Castelló-Pedrero, L., M. I. Gómez-Gómez, D. Zurita, J. García-Rupérez, A. Griol, and A. Martínez, "1310 nm TM grating couplers to operate silicon nitride ring resonator biosensors," *Results in Optics*, Vol. 11, 100418, May 2023.

[23] Doerr, C. R., L. Chen, Y.-K. Chen, and L. L. Buhl, "Wide bandwidth silicon nitride grating coupler," *IEEE Photonics Technology Letters*, Vol. 22, No. 19, 1461–1463, Oct. 2010.

[24] Zhang, H., C. Li, X. Tu, X. Luo, M. Yu, and P. G.-Q. Lo, "High efficiency silicon nitride grating coupler," *Applied Physics A*, Vol. 115, No. 1, 79–82, 2014.

[25] Zhao, X., D. Li, C. Zeng, G. Gao, Z. Huang, Q. Huang, Y. Wang, and J. Xia, "Compact grating coupler for 700-nm silicon nitride strip waveguides," *Journal of Lightwave Technology*, Vol. 34, No. 4, 1322–1327, Feb. 2016.

[26] Korček, R., D. M. Quiroz, Q. Wilmart, S. Edmond, P. Cheben, L. Vivien, C. Alonso-Ramos, and D. Benedikovič, "Library of single-etch silicon nitride grating couplers for low-loss and fabrication-robust fiber-chip interconnection," *Scientific Reports*, Vol. 13, No. 1, 17467, Oct. 2023.

[27] Fraser, W., R. Korček, D. Benedikovič, C. Horvath, S. Wang, and M. Vachon, "Single-etch silicon nitride grating couplers for multiband applications in quantum and fiber communications," *IEEE Journal of Selected Topics in Quantum Electronics*, Vol. 31, No. 5, 1–10, Sep.–Oct. 2025.

[28] Zhang, C., J.-H. Sun, X. Xiao, W.-M. Sun, X.-J. Zhang, T. Chu, J.-Z. Yu, and Y.-D. Yu, "High efficiency grating coupler for coupling between single-mode fiber and SOI waveguides," *Chinese Physics Letters*, Vol. 30, No. 1, 014207, 2013.

[29] Marchetti, R., C. Lacava, A. Khokhar, X. Chen, I. Cristiani, D. J. Richardson, G. T. Reed, P. Petropoulos, and P. Minzioni, "High-efficiency grating-couplers: Demonstration of a new design strategy," *Scientific Reports*, Vol. 7, No. 1, 16670, Nov. 2017.

[30] Chen, Y., T. D. Bucio, A. Z. Khokhar, M. Banakar, K. Grabska, F. Y. Gardes, R. Halir, I. Molina-Fernández, P. Cheben, and J.-J. He, "Experimental demonstration of an apodized-imaging chip-fiber grating coupler for Si_3N_4 waveguides," *Optics Letters*, Vol. 42, No. 18, 3566–3569, Sep. 2017.

[31] Lomonte, E., M. Stappers, L. Krämer, W. H. P. Pernice, and F. Lenzini, "Scalable and efficient grating couplers on low-index photonic platforms enabled by cryogenic deep silicon etching," *Scientific Reports*, Vol. 14, No. 1, 4256, Feb. 2024.

[32] Nambiar, S., P. Ranganath, R. Kallega, and S. K. Selvaraja, "High efficiency DBR assisted grating chirp generators for silicon nitride fiber-chip coupling," *Scientific Reports*, Vol. 9, No. 1, 18821, Dec. 2019.

[33] Zhang, H., C. Li, X. Tu, J. Song, H. Zhou, X. Luo, Y. Huang, M. Yu, and G. Lo, "Efficient silicon nitride grating coupler with distributed Bragg reflectors," *Optics Express*, Vol. 22, No. 18, 21 800–21 805, Sep. 2014.

[34] Nambiar, S., A. Kumar, R. Kallega, P. Ranganath, and S. K. Selvaraja, "High-efficiency grating coupler in 400 nm and 500 nm PECVD silicon nitride with bottom reflector," *IEEE Photonics Journal*, Vol. 11, No. 5, 1–13, Oct. 2019.

[35] Rawat, P., S. Nambiar, P. Venkatachalam, R. Singh, and S. K. Selvaraja, "Embedded silicon gratings for high-efficiency light-chip coupling to thin film silicon nitride waveguides," *Optics Express*, Vol. 31, No. 18, 29 392–29 402, Aug. 2023.

[36] Hong, J., A. M. Spring, F. Qiu, and S. Yokoyama, "A high efficiency silicon nitride waveguide grating coupler with a multilayer bottom reflector," *Scientific Reports*, Vol. 9, No. 1, 12988, Sep. 2019.

[37] Nambiar, S., A. Chatterjee, and S. K. Selvaraja, "Comprehensive grating enabled silicon nitride fiber-chip couplers in the SNIR wavelength band," *Optics Express*, Vol. 30, No. 3, 4327–4341, Jan. 2022.

[38] Chen, Y., R. Halir, I. Molina-Fernández, P. Cheben, and J.-J. He, "High-efficiency apodized-imaging chip-fiber grating coupler for silicon nitride waveguides," *Optics Letters*, Vol. 41, No. 21, 5059–5062, 2016.

[39] Benedikovic, D., C. Alonso-Ramos, D. Pérez-Galacho, S. Guerber, V. Vakarin, G. Marcaud, X. Le Roux, E. Cassan, D. Marris-Morini, P. Cheben, *et al.*, "L-shaped fiber-chip grating couplers with high directionality and low reflectivity fabricated with deep-UV lithography," *Optics Letters*, Vol. 42, No. 17, 3439–3442, 2017.

[40] Benedikovic, D., C. Alonso-Ramos, S. Guerber, X. Le Roux, P. Cheben, C. Dupre, B. Szelag, D. Fowler, E. Cassan, D. Marris-Morini, *et al.*, "Sub-decibel silicon grating couplers based on L-shaped waveguides and engineered subwavelength metamaterials," *Optics Express*, Vol. 27, No. 18, 26 239–26 250, Sep. 2019.

[41] Sacher, W. D., Y. Huang, G.-Q. Lo, and J. K. S. Poon, "Multilayer silicon nitride-on-silicon integrated photonic platforms and devices," *Journal of Lightwave Technology*, Vol. 33, No. 4, 901–910, Feb. 2015.

[42] Hosseinnia, A. H., A. H. Atabaki, A. A. Eftekhar, and A. Adibi, "High-quality silicon on silicon nitride integrated optical platform with an octave-spanning adiabatic interlayer coupler," *Optics Express*, Vol. 23, No. 23, 30 297–30 307, Nov. 2015.

[43] Sacher, W. D., Y. Huang, L. Ding, B. J. F. Taylor, H. Jayatilleka, G.-Q. Lo, and J. K. S. Poon, "Wide bandwidth and high coupling efficiency Si_3N_4-on-SOI dual-level grating coupler," *Optics Express*, Vol. 22, No. 9, 10 938–10 947, 2014.

[44] Xu, P., Y. Zhang, Z. Shao, L. Liu, L. Zhou, C. Yang, Y. Chen, and S. Yu, "High-efficiency wideband SiNx-on-SOI grating coupler with low fabrication complexity," *Optics Letters*, Vol. 42, No. 17, 3391–3394, 2017.

[45] Mak, J. C. C., Q. Wilmart, S. Olivier, S. Menezo, and J. K. S. Poon, "Silicon nitride-on-silicon bi-layer grating couplers designed by a global optimization method," *Optics Express*, Vol. 26, No. 10, 13 656–13 665, May 2018.

[46] Ong, E. W., N. M. Fahrenkopf, and D. D. Coolbaugh, "SiNx bilayer grating coupler for photonic systems," *OSA Continuum*, Vol. 1, No. 1, 13–25, Sep. 2018.

[47] Mak, J. C. C., W. D. Sacher, H. Ying, X. Luo, P. G.-Q. Lo, and J. K. S. Poon, "Multi-layer silicon nitride-on-silicon polarization-independent grating couplers," *Optics Express*, Vol. 26, No. 23, 30 623–30 633, Nov. 2018.
[48] Korček, R., P. Cheben, W. Fraser, J. H. Schmid, M. Milanizadeh, C. Alonso-Ramos, W. N. Ye, and D. Benedikovič, "Low-loss grating coupler based on inter-layer mode interference in a hybrid silicon nitride platform," *Optics Letters*, Vol. 48, No. 15, 4017–4020, Jul. 2023.
[49] Fraser, W., R. Korček, I. Glesk, J. Litvik, J. H. Schmid, P. Cheben, W. N. Ye, and D. Benedikovic, "High-efficiency metamaterial-engineered grating couplers for silicon nitride photonics," *Nanomaterials*, Vol. 14, No. 7, 581, Mar. 2024.
[50] Fraser, W., D. Benedikovic, R. Korcek, M. Milanizadeh, D.-X. Xu, J. H. Schmid, P. Cheben, and W. N. Ye, "High-efficiency self-focusing metamaterial grating coupler in silicon nitride with amorphous silicon overlay," *Scientific Reports*, Vol. 14, No. 1, 11651, May 2024.
[51] Kohli, M., D. Chelladurai, B. Vukovic, D. Moor, D. Bisang, K. Keller, A. Messner, T. Buriakova, M. Zervas, Y. Fedoryshyn, U. Koch, and J. Leuthold, "C- and O-band dual-polarization fiber-to-chip grating couplers for silicon nitride photonics," *ACS Photonics*, Vol. 10, No. 9, 3366–3373, Aug. 2023.
[52] Vitali, V., C. Lacava, T. D. Bucio, F. Y. Gardes, and P. Petropoulos, "Highly efficient dual-level grating couplers for silicon nitride photonics," *Scientific Reports*, Vol. 12, No. 1, 15436, Sep. 2022.
[53] Chmielak, B., S. Suckow, J. Parra, V. C. Duarte, T. Mengual, M. A. Piqueras, A. L. Giesecke, M. C. Lemme, and P. Sanchis, "High-efficiency grating coupler for an ultralow-loss Si_3N_4-based platform," *Optics Letters*, Vol. 47, No. 10, 2498–2501, May 2022.
[54] Jung, H., M.-J. Kwack, and Y. Kim, "Simulation study of a highly efficient dual-apodized a-Si/SiN grating coupler using a metal bottom reflector on a glass substrate for co-packaged optics," *Japanese Journal of Applied Physics*, Vol. 64, No. 9, 092001, Sep. 2025.
[55] *Ansys Lumerical FDTD*, [Online]. Available: https://www.lumerical.com/ansys/, 2024.
[56] Van Laere, F., T. Claes, J. Schrauwen, S. Scheerlinck, W. Bogaerts, D. Taillaert, L. O'Faolain, D. Van Thourhout, and R. Baets, "Compact focusing grating couplers for silicon-on-insulator integrated circuits," *IEEE Photonics Technology Letters*, Vol. 19, No. 23, 1919–1921, Dec. 2007.
[57] Reed, G. T. and A. P. Knights, *Silicon Photonics: An Introduction*, John Wiley & Sons, Hoboken, NJ, 2004.
[58] Floquet, G., "Sur les équations différentielles linéaires à coefficients périodiques," *Annales Scientifiques de l'École Normale Supérieure*, Vol. 12, 47–88, 1883.
[59] Bloch, F., "Über die quantenmechanik der elektronen in Kristallgittern," *Zeitschrift für Physik*, Vol. 52, No. 7, 555–600, Jul. 1929.
[60] Orobtchouk, R., A. Layadi, H. Gualous, D. Pascal, A. Koster, and S. Laval, "High-efficiency light coupling in a submicrometric silicon-on-insulator waveguide," *Applied Optics*, Vol. 39, No. 31, 5773–5777, Nov. 2000.
[61] Bates, K. A., L. Li, R. L. Roncone, and J. J. Burke, "Gaussian beams from variable groove depth grating couplers in planar waveguides," *Applied Optics*, Vol. 32, No. 12, 2112–2116, Apr. 1993.
[62] Cheben, P., R. Halir, J. H. Schmid, H. A. Atwater, and D. R. Smith, "Subwavelength integrated photonics," *Nature*, Vol. 560, No. 7720, 565–572, Aug. 2018.
[63] Cheben, P., J. H. Schmid, R. Halir, J. M. Luque-González, J. G. Wangüemert-Pérez, D. Melati, and C. Alonso-Ramos, "Recent advances in metamaterial integrated photonics," *Advances in Optics and Photonics*, Vol. 15, No. 4, 1033–1105, Dec. 2023.
[64] Halir, R., P. J. Bock, P. Cheben, A. Ortega-Moñux, C. Alonso-Ramos, J. H. Schmid, J. Lapointe, D.-X. Xu, J. G. Wangüemert-Pérez, I. Molina-Fernández, and S. Janz, "Waveguide subwavelength structures: A review of principles and applications," *Laser & Photonics Reviews*, Vol. 9, No. 1, 25–49, Jan. 2015.
[65] Rytov, S., "Electromagnetic properties of a finely stratified medium," *Soviet Physics JEPT*, Vol. 2, 466–475, May 1956.
[66] Raguin, D. H. and G. M. Morris, "Antireflection structured surfaces for the infrared spectral region," *Applied Optics*, Vol. 32, No. 7, 1154–1167, Mar. 1993.
[67] Benedikovic, D., C. Alonso-Ramos, P. Cheben, J. H. Schmid, S. Wang, D.-X. Xu, J. Lapointe, S. Janz, R. Halir, A. Ortega-Moñux, J. G. Wangüemert-Pérez, I. Molina-Fernández, J.-M. Fédéli, L. Vivien, and M. Dado, "High-directionality fiber-chip grating coupler with interleaved trenches and subwavelength index-matching structure," *Optics Letters*, Vol. 40, No. 18, 4190–4193, Sep. 2015.
[68] Benedikovic, D., P. Cheben, J. H. Schmid, D.-X. Xu, J. Lapointe, S. Wang, R. Halir, A. Ortega-Moñux, S. Janz, and M. Dado, "High-efficiency single etch step apodized surface grating coupler using subwavelength structure," *Laser & Photonics Reviews*, Vol. 8, No. 6, L93–L97, Nov. 2014.
[69] Halir, R., P. Cheben, S. Janz, D.-X. Xu, I. Molina-Fernández, and J. G. Wangüemert-Pérez, "Waveguide grating coupler with subwavelength microstructures," *Optics Letters*, Vol. 34, No. 9, 1408–1410, 2009.
[70] Wang, Y., H. Yun, Z. Lu, R. Bojko, W. Shi, X. Wang, J. Flueckiger, F. Zhang, M. Caverley, N. A. F. Jaeger, and L. Chrostowski, "Apodized focusing fully etched subwavelength grating couplers," *IEEE Photonics Journal*, Vol. 7, No. 3, 1–10, Jun. 2015.
[71] Oton, C. J., "Long-working-distance grating coupler for integrated optical devices," *IEEE Photonics Journal*, Vol. 8, No. 1, 1–8, Feb. 2016.
[72] Ferrari, A., A. Napoli, J. K. Fischer, N. Costa, A. D'Amico, J. Pedro, W. Forysiak, E. Pincemin, A. Lord, A. Stavdas, *et al.*, "Assessment on the achievable throughput of multi-band ITU-T G.652.D fiber transmission systems," *Journal of Lightwave Technology*, Vol. 38, No. 16, 4279–4291, Aug. 2020.
[73] Dabos, G., A. Manolis, A. L. Giesecke, C. Porschatis, B. Chmielak, T. Wahlbrink, N. Pleros, and D. Tsiokos, "TM grating coupler on low-loss LPCVD based Si_3N_4 waveguide platform," *Optics Communications*, Vol. 405, 35–38, Dec. 2017.